Dosimetric accuracy of proton therapy for chordoma patients with titanium implants

Joost M. Verburg[a)]
Department of Radiation Oncology, Massachusetts General Hospital and Harvard Medical School, Boston, Massachusetts 02114 and School of Medical Physics and Engineering, Eindhoven University of Technology, Eindhoven, The Netherlands

Joao Seco
Department of Radiation Oncology, Massachusetts General Hospital and Harvard Medical School, Boston, Massachusetts 02114

(Received 7 January 2013; revised 11 April 2013; accepted for publication 22 May 2013; published 25 June 2013)

Purpose: To investigate dosimetric errors in proton therapy treatment planning due to titanium implants, and to determine how these affect postoperative passively scattered proton therapy for chordoma patients with orthopedic hardware.
Methods: The presence of titanium hardware near the tumor may affect the dosimetric accuracy of proton therapy. Artifacts in the computed tomography (CT) scan can cause errors in the proton stopping powers used for dose calculation, which are derived from CT numbers. Also, clinical dose calculation algorithms may not accurately simulate proton beam transport through the implants, which have very different properties as compared to human tissue. The authors first evaluated the impact of these two main issues. Dose errors introduced by metal artifacts were studied using phantoms with and without titanium inserts, and patient scans on which a metal artifact reduction method was applied. Pencil-beam dose calculations were compared to models of nuclear interactions in titanium and Monte Carlo simulations. Then, to assess the overall impact on treatment plans for chordoma, the authors compared the original clinical treatment plans to recalculated dose distributions employing both metal artifact reduction and Monte Carlo methods.
Results: Dose recalculations of clinical proton fields showed that metal artifacts cause range errors up to 6 mm distal to regions affected by CT artifacts. Monte Carlo simulations revealed dose differences $>10\%$ in the high-dose area, and range differences up to 10 mm. Since these errors are mostly local in nature, the large number of fields limits the impact on target coverage in the chordoma treatment plans to a small decrease of dose homogeneity.
Conclusions: In the presence of titanium implants, CT metal artifacts and the approximations of pencil-beam dose calculations cause considerable errors in proton dose calculation. The spatial distribution of the errors however limits the overall impact on passively scattered proton therapy for chordoma. © *2013 American Association of Physicists in Medicine*. [http://dx.doi.org/10.1118/1.4810942]

Key words: proton therapy, radiation therapy, cancer, chordoma, implants, computed tomography, metal artifacts, metal artifact reduction, Monte Carlo methods, dosimetry, treatment planning

I. INTRODUCTION

Proton radiotherapy is often the modality of choice to deliver postoperative radiotherapy to patients with head and neck and spinal tumors that require high doses for tumor control, such as chordoma. The required doses often cannot be delivered using conventional radiotherapy due to the dose limits on the spinal cord or brain stem.

These patients frequently have titanium orthopedic hardware near the tumor site, which is needed to stabilize the vertebral column after surgery. The presence of implant materials can affect the accuracy of proton therapy treatment plans due to metal artifacts in the computed tomography (CT) scan[1,2] and the approximations of pencil-beam dose calculation methods.[3]

A recent clinical study of chordoma patients who received proton therapy, showed a significant association between the presence of titanium-based surgical stabilization and reduced tumor control.[4] Another study at our institution also reported a trend of local recurrence.[5] While many factors may be responsible, it warrants further investigation of dosimetric errors caused by this type of implant. Also, it is important to quantify the impact on clinical treatment plans, to establish if changes to these treatments are necessary and because concerns over the dosimetric errors have led to some institutions to decide not to treat these patients with proton therapy.

First, the impact of artifacts in the CT scan for treatment planning is studied. Titanium causes hardening of the CT x-rays, which typically results in streak artifacts in the reconstructed CT images. CT numbers are used to determine the proton stopping power of tissues in the beam path; artifacts can therefore result in errors in the calculated proton range. In clinical treatment plans, proton stopping powers may be manually changed to attempt to reduce these errors.[4] The

accuracy of such corrections is however uncertain, as it is difficult to manually determine anatomy and tissue density in images obscured by the artifacts.

Second, we investigate the accuracy of clinical pencil-beam dose calculations. Since these methods are based on water as a reference medium,[6] they may not accurately simulate beam transport through titanium, which has characteristics very different from water and normal tissues. In particular, elastic multiple Coulomb interactions with the nuclei and nonelastic nuclear reactions are specific to each element. Multiple Coulomb scattering is relevant as it results in a local widening of the proton beam. Nonelastic interactions cause a loss of the primary proton fluence, which affects the downstream dose delivery.

Then, to assess the clinical impact of the dosimetric errors, we evaluate in retrospect two treatment plans of chordoma patients with titanium orthopedic hardware. The clinically planned dose distributions are compared to dose calculations that employ both CT metal artifact reduction and Monte Carlo methods to simulate the beam transport through the implants.

II. METHODS AND MATERIALS

II.A. Study design

The question we seek to answer is how CT metal artifacts and the approximations of the pencil-beam dose calculation method affect dose calculation accuracy in the presence of titanium implants. Also, we aim to quantify the impact of these potential dosimetric errors on clinical treatment plans for chordoma. The main issues under study are:

- CT metal artifacts due to the titanium implants.
- The simulation of beam transport through titanium, particularly:
  - Multiple Coulomb scattering of protons passing through implants.
  - Nonelastic nuclear interactions in implants.

II.A.1. CT metal artifacts

To assess the impact of CT metal artifacts, we first studied a treatment plan designed on a phantom CT scan in which a severe metal artifact was created using titanium inserts. The purpose of this study was to determine the extent of proton range errors that can potentially be introduced by the CT artifacts.

The phantom was scanned with and without titanium inserts. Proton beams were planned to pass through different parts of the artifacts, with the spread-out Bragg peak (SOBP) targeted on a cylindrical volume. Using the pencil-beam dose calculation algorithm, the doses delivered by the beams were calculated on both the artifact-affected CT scans and ground truth scans without titanium inserts. We analyzed the dose distributions of three proton beams passing through different parts of the metal artifact.

The effect of artifacts on clinical proton beams was studied by recalculating dose distributions on artifact-reduced CT images. Sinograms of patient treatment planning scans were acquired from the CT scanner and a previously developed CT metal artifact reduction method was applied.[7] Although no current method can completely eliminate all metal artifacts, our method significantly reduces the artifacts, providing reconstructed CT images that better reflect the actual patient anatomy.

II.A.2. Beam transport through titanium

The second part of the study involves an analysis of the accuracy of pencil-beam dose calculations with respect to the calculation of beam transport through titanium implants. Pencil-beam dose calculation algorithms use measured depth–dose curves in water as input data, rather than using more fundamental physical principles. Therefore, although the energy loss of protons due to the titanium implant is taken into account, most pencil-beam algorithms do not incorporate effects specific to the structure of the titanium nucleus. Essentially, it is assumed that titanium can be represented by a virtual high-density water medium.

To better understand the errors introduced by these approximations, we studied nonelastic nuclear reactions and multiple Coulomb scattering of protons passing through titanium. The fluence loss because of nonelastic nuclear reactions was calculated, and the root-mean-square (RMS) scattering angles due to multiple Coulomb interactions were determined. These results were compared to calculations using water with a stopping power equivalent to titanium.

To quantify the effects on dose calculation, a Monte Carlo simulation of a proton beam was performed on a computational phantom with a titanium cylinder, and compared to the results of a pencil-beam calculation. Finally, Monte Carlo simulations of clinical proton beams were performed, using the artifact-reduced CT images.

II.A.3. Evaluation of chordoma treatment plans

To determine the impact of the implants on clinical treatment plans for chordoma, we combined the CT metal artifact reduction algorithm and Monte Carlo dose calculation methods to recalculate in retrospect the treatment plans of two patients. The original dose distributions were compared to the corrected dose calculations, and dose–volume histogram (DVH) analysis was performed.

II.B. CT scans

II.B.1. Phantom scan

A Gammex 467 tissue characterization phantom (Gammex Inc., Middleton, WI) was scanned on a GE LightSpeed RT 16 CT scanner (GE Healthcare, Waukesha, WI) with a 140 kV x-ray tube voltage and a current of 600 mA (see Fig. 1). These imaging parameters are similar to those used at our institution for patients with titanium implants.

Two titanium cylinders with a diameter of 25.4 mm were placed in the phantom perpendicular to the transverse plane. A second scan without titanium inserts was performed to serve

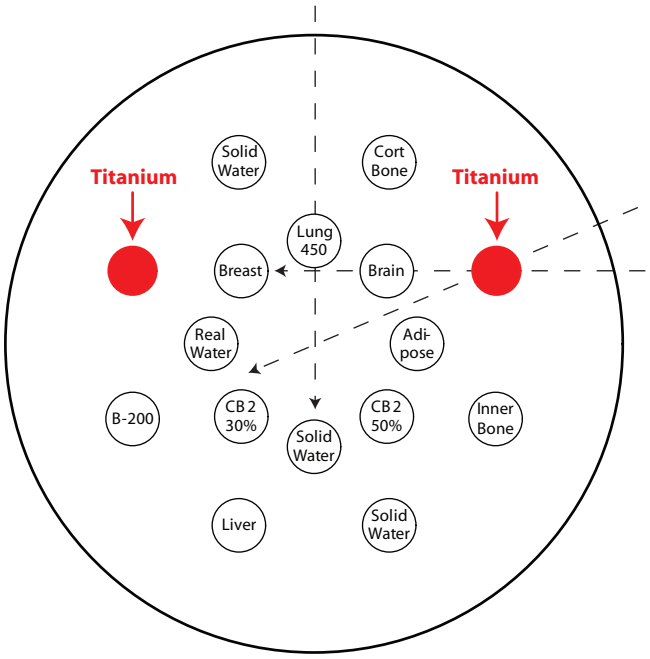

FIG. 1. Cross section of the tissue characterization phantom used to study CT metal artifacts. The phantom consists of a disk of solid water in which various tissue-equivalent plastics are inserted. One scan was obtained with two titanium cylinders in the positions indicated; a second ground truth scan was acquired without the titanium cylinders. The dashed lines indicate the beam angles used in the study.

as ground truth. To the images of the ground truth scan, virtual titanium inserts were added with the exact size and location of the real inserts.

II.B.2. Patient scans

The CT scans of two chordoma patients were studied in retrospect. Both patients had titanium constructs that were used to stabilize the vertebral column, and were connected by cross links. Details of the patient scans are listed in Table I. The patients were scanned on the same GE LightSpeed RT 16 scanner in axial mode. Sinograms were obtained from the scanner, and using the scanner system were calibrated and rebinned to parallel-bin geometry.

The CT metal artifact reduction algorithm used is described in more detail in our previous work.[7] Metal artifacts due to the titanium stabilization hardware were reduced by a physics correction algorithm which employs a beam hardening correction. This method compares the projections through titanium with neighboring projections not passing through the implants, creating a first-order model of beam hardening which was used to adjust the values of projections passing through the hardware. The locations of the titanium implants were determined using a threshold of 2500 Hounsfield units (HU) on the CT numbers in the original image reconstruction. Any voxels with a CT number above this threshold were considered to comprise the implants. This segmentation of the titanium implants was validated using CT projections rebinned into virtual radiographs, which are not affected by metal artifacts.

Artifacts due to high-Z implants (such as dental fillings), or a combination of high-Z implants and titanium hardware, were further reduced using an iterative optimization algorithm that replaces missing projections caused by near-complete x-ray attenuation. In this case, a higher

TABLE I. Details of the clinical CT scans and treatment plans.

	Patient 1	Patient 2
Body site	Lumbar spine	Cervical spine
Treatment position	Head-first prone	Head-first supine
Ti hardware	Four rods, cage, cross links	Three rods, cage, cross links
Other hardware	None	Dental fillings
Prescribed dose (postoperative)	39.6 Gy RBE	48.6 Gy RBE
Total dose	70.2 Gy RBE	75.6 Gy RBE
Proton beams	• Three uniform fields • Two patch/through field combinations	• Four uniform fields • Four patch/through field combinations
	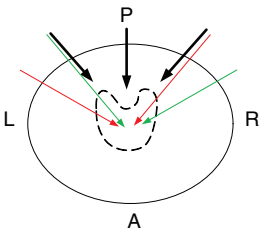	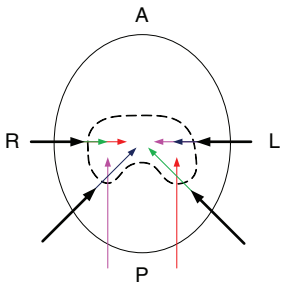
	Black lines: uniform fields; colored lines: patch/through field combinations	
CT scan	• 140 kV tube voltage • 565 mA current • 2.5 mm slice thickness • 2 s rotation	• 140 kV tube voltage • 590 mA current • 2.5 mm slice thickness • 1 s rotation

threshold of 8000 HU was used to identify the high-Z implants.

II.C. Treatment planning

The treatment plans we studied were designed for passively scattered proton therapy delivery, and were created using the XiO (Elekta AB, Stockholm, Sweden) treatment planning system (TPS). All radiation doses are reported in Gy RBE (relative biological effectiveness), using the conventional constant proton RBE of 1.1.

II.C.1. Phantom for metal artifacts study

The treatment plan designed on the tissue characterization phantom, which was used to study metal artifacts, consisted of three coplanar proton beams passing through different parts of the main metal artifact between the two titanium cylinders. Two beams targeted a cylinder at the center of the phantom, entering the phantom, respectively, from the top and at a right oblique 67° angle (refer Fig. 1). A third beam was oriented parallel to the two titanium inserts and targeted a cylinder in the middle of the inserts. All target volumes had a diameter of 5 cm.

II.C.2. Phantom for dose calculation study

To assess calculations of proton beam transport through titanium, a treatment plan was created on a virtual water phantom with a titanium cylinder. The plan featured a single beam designed to target a cylindrical region (5 cm diameter) located 10 cm distal to a titanium cylinder with a diameter of 1 cm. The titanium cylinder was placed 5 cm from the surface of the phantom. The doses were calculated on a high-resolution grid with 0.65 mm^3 voxels.

II.C.3. Patient treatment plans

The clinical treatment plans analyzed in this work were created for the postoperative proton radiotherapy received by the chordoma patients. The patients also received preoperative radiotherapy; this part of the treatment is however not relevant for the present study because the titanium implants were not yet present. The prescription doses and beam arrangements are provided in Table I.

The clinical treatment plans used several uniform beams combined with patch and through beams to spare the nearby spinal cord. This beam arrangement combines a through beam which delivers dose to the majority of the tumor with a patch field that is laterally conformed to the transverse edge of the through beam, and delivers dose to the remaining part of the target next to the critical tissue.[8] Dose calculations were performed with a 2 mm^3 voxel size.

Treatment plans for passively scattered proton therapy at our institution are designed to be robust against a ±3.5% variation of the water-equivalent range in the patient.[8] This margin is necessary because of various uncertainties, mainly related to the errors and degeneracy in the conversion of CT x-ray attenuation to proton stopping powers.[9] In addition, depending on the tumor site, a certain smearing of the range compensator is employed to ensure robustness against patient motion.[10] There is currently no standard to include additional margins when metallic implants are present.

II.D. Pencil-beam dose calculation algorithm

The pencil-beam dose calculation method is an implementation of the Hong *et al.*[6] algorithm. The broad proton beam is modeled as a combination of small computational pencil-beams for which the transport through the range compensator and patient is analytically calculated. Measured depth–dose curves in water for various energies and configurations of the treatment head provide the principal physical input parameters.

The energy loss of protons is simulated as a loss in residual proton range by considering the stopping power of the compensator and tissues relative to water, which is almost constant over the therapeutic energy range. Multiple Coulomb scattering is incorporated by increasing the radial emittance of the protons in a Gaussian approximation, using the generalized Highland[11] formula as described by Gottschalk *et al.*[12] Material-specific properties are used to model multiple Coulomb scattering in the range compensator. In the patient, multiple Coulomb scattering is simulated assuming the tissue upstream in the beam path consists of a volume of water with the same integral proton stopping power as the tissue. Therefore, neither the scattering properties of titanium, nor the position of the titanium implants in the path of the pencil-beam is included.

II.E. Monte Carlo simulations

Monte Carlo dose calculations were performed with the TOPAS Monte Carlo code[13] using the Geant4 9.5.p01 toolkit.[14] TOPAS is a Monte Carlo code currently under development, which will be released to the proton therapy community in the near future. Our in-house MCAUTO code directly links the XiO TPS to this Monte Carlo simulation framework. All proton beam configurations and associated apertures and range compensators are automatically obtained from the planning system.

II.E.1. Treatment head

Unlike the pencil-beam algorithm, which uses measured depth–dose profiles in water as input parameters, the Monte Carlo code requires complete phase space information of the proton beams to perform patient dose calculations. These phase space data were generated by simulating the proton transport through the treatment head and the field-specific aperture and range compensator.

Proton beams in the XiO TPS are prescribed a beam weight, which is defined as the dose that would be delivered by said beam to water in the SOBP region, if the center of the SOBP is at isocenter. For each field, the relationship between the beam weight and the number of protons at the

entrance of the treatment head was determined by performing a separate Monte Carlo output factor simulation, taking into account the effects of the air gap and the size of the aperture opening.

II.E.2. Patient anatomy

Particle transport through the patient anatomy was simulated based on the treatment planning CT scan. The range of CT numbers was divided in 24 bins, which were each assigned a different elemental composition following the results of Schneider *et al.*[15] In addition, CT numbers above 2500 HU were considered to comprise the titanium implants and were modeled as pure titanium in the Monte Carlo simulation.

A unique mass density was assigned to each CT number. This was determined by matching the relative proton stopping powers as determined by the Monte Carlo code with the relative stopping power used by the XiO TPS, which was calibrated to the CT scanners used at our department. This method ensures consistency between the assumptions in the pencil-beam dose calculation and the Monte Carlo simulations. In homogeneous media, the proton range as determined using the Monte Carlo code matches the clinical pencil-beam dose calculation within 1 mm.

An on-the-fly conversion was performed to convert the Monte Carlo simulated dose to dose-to-water, which is the measure of dose reported by pencil-beam algorithms that are conventionally used in radiotherapy.[16]

II.E.3. Physics models

The Geant4 physics models used have been validated for proton therapy simulation at our institution, and are also the default models used in TOPAS. Electromagnetic interactions were simulated using the Geant4 standard EM model with the high-precision option enabled, which increases the resolution of the stopping power tables. For protons, the UrbanMsc90 multiple Coulomb scattering model was used. This model uses a modified Highland[11] formula for the angular distribution of the scattering, combined with an empirical function for the non-Gaussian tail. Nonelastic proton–nucleus interactions were simulated with the binary cascade model at higher proton energies, followed by the precompound and evaporation model. The default Wellisch-Axen parametrization of the total noneleastic nuclear reaction cross sections was employed.[17]

II.E.4. Physics model validation

We performed a number of validations of the Geant4 physics models to ensure accurate simulation of proton interactions with titanium. The parametrization of the total nonelastic reaction cross section used by Geant4, which is the main parameter determining the loss of proton fluence distal to titanium implants, was compared to experimental data in the 9–100 MeV incident proton energy range[18–21] as compiled by Bauhoff.[22] Comparisons were also made to optical model calculations using the TALYS 1.4 nuclear reaction code.[23] TALYS incorporates the ECIS-06 optical model code, which was used with the Koning and Delaroche[24] global optical model potential.

No experimental data of proton multiple Coulomb scattering in titanium were found in literature for the relevant energy range. We therefore compared Gaussian profiles fitted to the radial proton emittance in Geant4 simulations with Gaussian fits to Molière theory.[25] Molière theory was shown to have good accuracy for other intermediate-Z materials.[12] The Molière theory evaluations were performed using the BGware code .[26] We used the method of Hanson *et al.*[27] to convert the characteristic scattering angle obtained using Molière theory to a Gaussian approximation.

Geant4 simulations of multiple Coulomb scattering were performed by transporting protons through a slab of material. The incident protons were orientated perpendicular to this slab, and their angular momentum was registered after passing through the slab. A Gaussian distribution was fitted to the angular distribution of the outgoing protons by minimizing the least-square error. Simulations were performed with initial proton energies of 100, 150, and 200 MeV and titanium slabs of 5, 10, 15, and 20 mm thickness.

II.F. Proton–nuclear interactions with titanium

The difference between a pencil-beam dose calculation and a Monte Carlo simulation is a superposition of several effects that are better accounted for in the Monte Carlo models. To determine the magnitude of these effects, we performed several simulations in simple geometries, in which nuclear interactions with titanium were compared to a model in which the titanium is represented by water with an equivalent proton stopping power. Multiple Coulomb scattering was simulated in Geant4 using the same approach as described in Sec. II.E.4. In addition, fluence loss due to nonelastic nuclear interactions was calculated using the total nonelastic reactions cross sections obtained from Geant4.

III. RESULTS

III.A. Impact of metal artifacts

III.A.1. Phantom study

We show in Fig. 2 the impact of a severe metal artifact on the phantom dose calculation. The presence of two titanium cylinders results in bright and dark streaks in the CT images; the artifacts mostly appear between the cylinders and between the titanium and other tissue equivalent materials with higher densities.

As expected, the impact of the artifacts depends on the orientation of the proton beam. The proton range errors varied between 1 and 10 mm. Because of the severe metal artifact in this phantom study, the impact on the clinical proton beams would normally be expected to be within this range.

The dose calculation of a beam oriented perpendicular to several bright and dark artifacts is almost unaffected by the

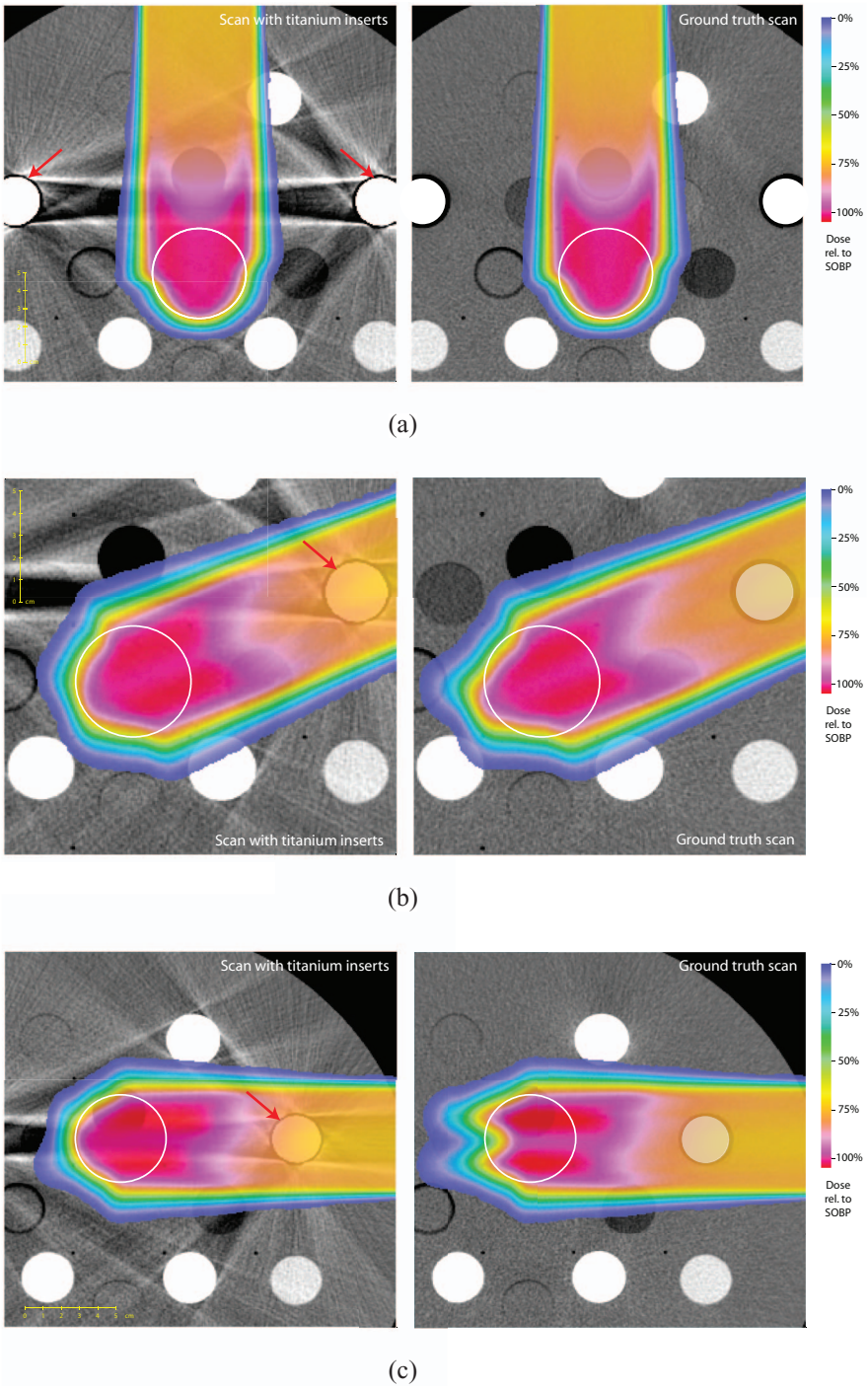

FIG. 2. Phantom dose calculations of three proton beams passing through different parts of a metal artifact. The dose is calculated on the artifact-affected CT scan with titanium cylinders and the ground truth scans without artifacts. The ground truth scan includes a virtual titanium cylinder matching the physical one. Doses below 0.5% of the SOBP dose are not shown. CT window level: 40 HU and window width: 400 HU. (a) Beam perpendicular to main artifact; (b) beam through one titanium insert; and (c) beam parallel to main artifact.

artifacts, as seen in Fig. 2(a). The small effect on the calculated range can be explained by the fact that errors due to several bright and dark streak artifacts cancel out.

Shown in Fig. 2(b) is a beam coming from an oblique angle, which passes through the cylinder itself and the bright artifacts surrounding it. In this case, the recalculation of the dose on the ground truth scan shows an increase of the range in the central beam axis by about 5 mm.

Finally, in Fig. 2(c), the beam is oriented parallel to the main metal artifact. In this worst-case situation, range shifts on the order of 10 mm are observed in both directions.

III.A.2. Patient study

The originally planned dose distributions of the fields for the chordoma patients were recalculated on artifact-reduced

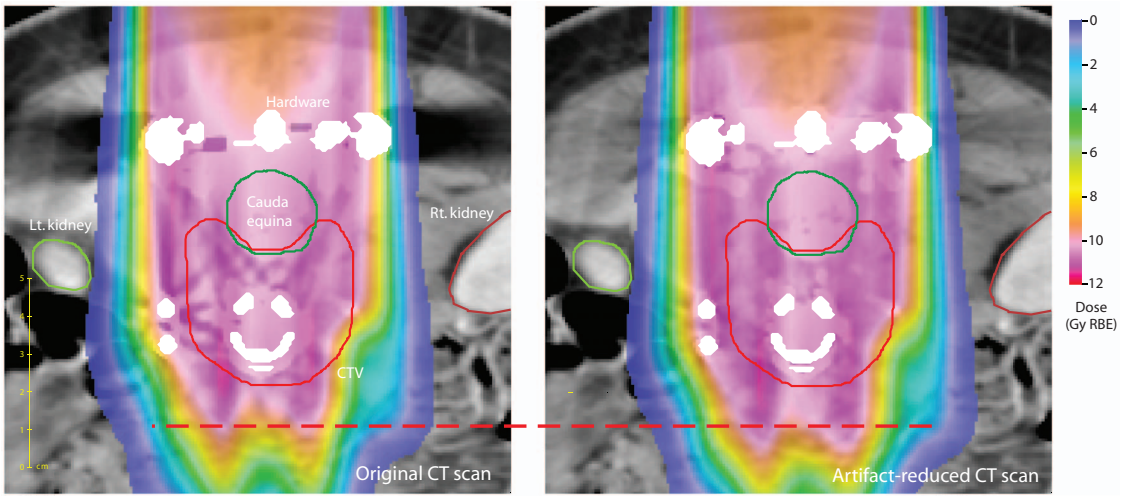

FIG. 3. Dose calculations of a posterior–anterior proton beam passing through titanium hardware in the lumbar spine. The dashed line near the end-of-range of the beam is drawn to guide the eye. Doses below 0.1 Gy RBE are not shown. CT window level: 40 HU and window width: 400 HU.

CT images. In both patient cases, the recalculated dose distributions showed an increase of the proton range for the parts of the beams that passed through or near the titanium hardware. Target coverage therefore was not compromised. The maximum range overshoot was 6 mm in soft tissue at 80% dose level.

A cross section of the dose distribution for one of the proton beams of each treatment plan is shown in Figs. 3 and 4. The increase in range can clearly be seen in both cases. In the case of patient 2 (refer Fig. 4), the original beam was planned with the high-dose area just proximal to the parotid gland. The recalculated dose distribution shows this area shifted into the proximal side of the gland. This issue occurred to some extent in all left-right, right-left, and oblique beams.

III.B. Impact of dose calculation method

III.B.1. Geant4 physics model validation

In Fig. 5 and Table II, validations of the Geant4 models for the simulation of proton transport through titanium are presented.

First, shown in Fig. 5 is the total nonelastic cross section of proton-induced reactions on titanium (isotopes in natural abundance). The Geant4 9.5 cross sections are compared to a TALYS optical model calculation and experimental data. A good agreement is found between the models and measurement data. The uncertainty in the cross section is estimated to be below 10% for the clinical proton energy range. Since only a small fraction of the protons passing through an implant will undergo a nuclear reaction, this uncertainty has a very small impact on dose calculation.

A comparison was also made between the Geant4 simulations of multiple Coulomb scattering and Molière theory, the results of which are provided in Table II. The agreement of the RMS scattering angles is satisfactory with differences of only a few percent.

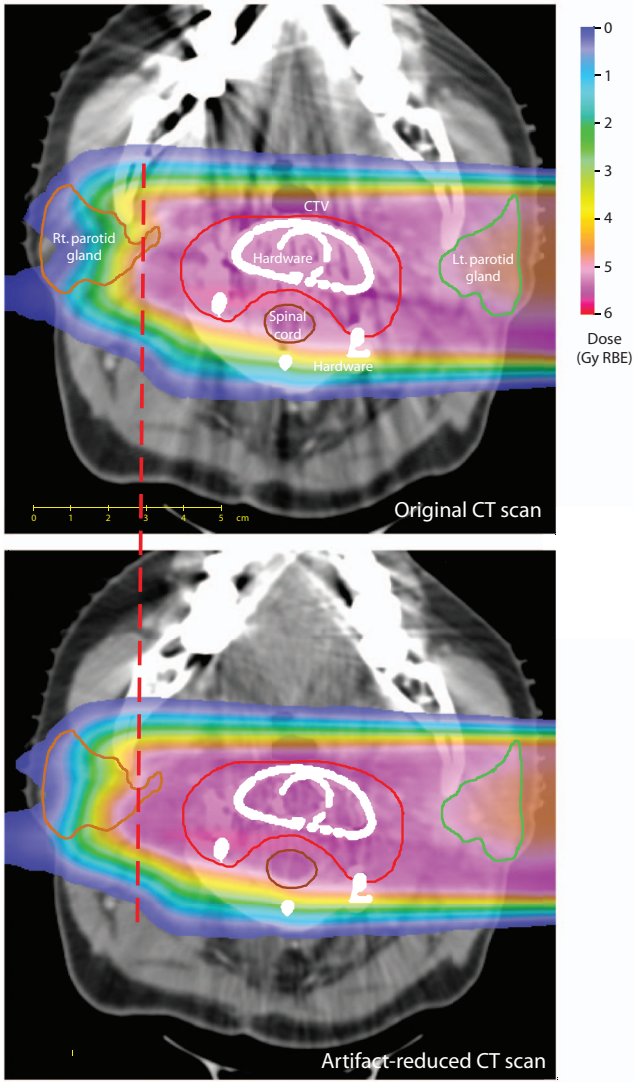

FIG. 4. Dose calculations of a proton beam around titanium hardware in the cervical spine. The dashed line near the end-of-range of the beam is drawn to guide the eye. Doses below 0.1 Gy RBE are not shown. CT window level: 40 HU and window width: 400 HU.

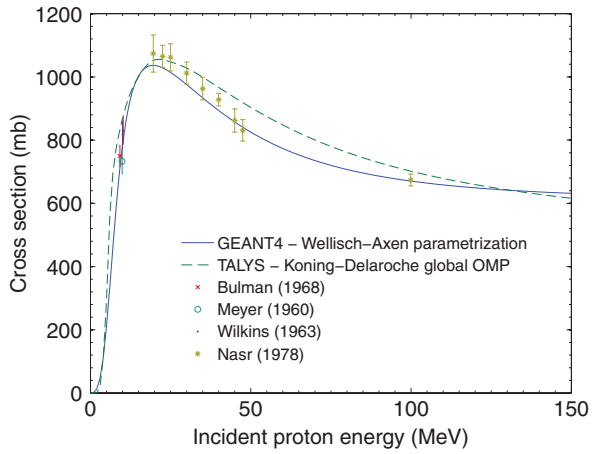

FIG. 5. Total nonelastic nuclear reaction cross section of proton-induced reactions on titanium.

III.B.2. Proton-nuclear interactions with titanium

Having validated the physics models, we analyzed how the approximations of the pencil-beam dose calculation algorithm differ from calculations specifically modeling the proton interactions with the titanium nuclei. Tabulated in Table III is the RMS multiple Coulomb scattering angle for various combinations of proton energy and titanium thickness, compared to the RMS angle if the medium is assumed to be water with the same stopping power as titanium. In all the cases, the water-based simulation underestimates the RMS scattering angle by approximately 50%. The approximation error therefore becomes greater with a larger amount of titanium in the beam path, or a lower proton energy, as both increase the multiple Coulomb scattering angle.

Depicted in Fig. 6 is the effect of nonelastic nuclear interactions. The proton fluence loss per cm of titanium in the water-based approximation is compared to a calculation using the cross sections for titanium (refer Fig. 5). At low incident proton energies, the water-based approximation is almost equivalent to the titanium cross section. The difference is somewhat larger in the case of higher energies but remains limited.

TABLE II. Comparison of Geant4 model predictions of proton multiple Coulomb scattering in titanium to Molière theory calculations. The RMS angle of Gaussian fits to the angular distributions is listed.

Ingoing proton energy (MeV)	Titanium thickness (mm)	RMS angle Molière theory (mrad)	RMS angle Geant4 (mrad)	Difference (%)
100	5	27.19	25.99	−4.41
100	10	42.05	41.03	−2.43
100	15	58.86	56.74	−3.60
100	20	80.24	77.96	−2.84
150	5	17.82	17.15	−3.76
150	10	26.90	25.91	−3.68
150	15	33.50	33.51	0.03
150	20	41.45	40.80	−1.57
200	5	13.28	12.98	−2.26
200	10	19.24	19.36	0.62
200	15	24.42	24.67	1.02
200	20	30.04	29.50	−1.80

TABLE III. Comparison of Geant4 simulations of multiple Coulomb scattering in titanium and a virtual high-density water medium with equivalent proton stopping power. The RMS angle of Gaussian fits to the angular distributions is listed.

Ingoing proton energy (MeV)	Titanium thickness (mm)	RMS angle Titanium (mrad)	RMS angle Water-based (mrad)	Difference (%)
100	5	25.99	13.31	−48.79
100	10	41.03	20.93	−48.99
100	15	56.74	28.89	−49.08
100	20	77.96	39.79	−48.96
150	5	17.15	8.80	−48.69
150	10	25.91	13.23	−48.94
150	15	33.51	17.06	−49.09
150	20	40.80	20.73	−49.19
200	5	12.98	6.67	−48.61
200	10	19.36	9.91	−48.81
200	15	24.67	12.58	−49.01
200	20	29.50	15.00	−49.15

III.B.3. Phantom study

From the previous findings, it follows that the pencil-beam model of multiple Coulomb scattering is the main issue that may result in dosimetric errors when titanium implants are present. To assess the impact on dosimetry, a comparison of a pencil-beam dose calculation and a Monte Carlo simulation on the virtual voxelized water phantom is shown in Fig. 7.

The Monte Carlo simulation shows a significantly larger reduction in dose delivered distal to the titanium cylinder. Also, elevated dose is seen distal to the edges of the titanium cylinder. For this particular geometry, the Monte Carlo

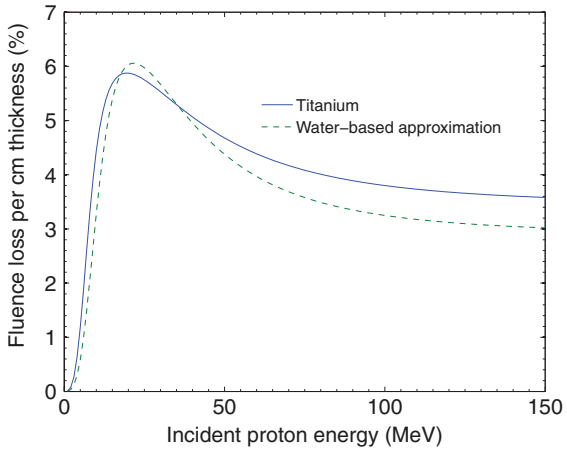

FIG. 6. Calculation of the loss of primary proton fluence due to nonelastic nuclear reaction in titanium, using the Wellisch and Axen (Ref. 17) parametrization. A calculation using the nonelastic reaction cross section of titanium is compared to a calculation based on the cross section for water scaled by the relative proton stopping power of titanium.

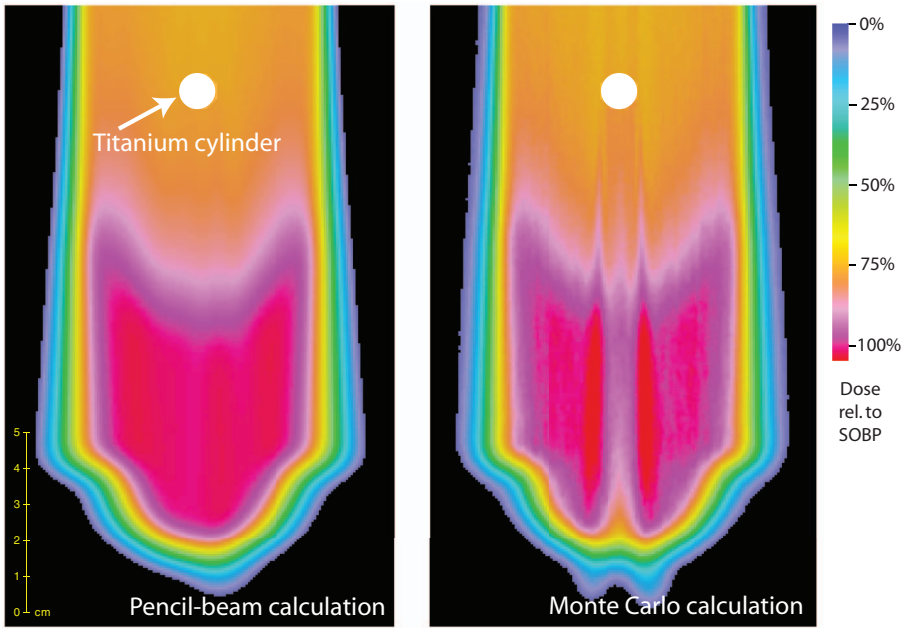

FIG. 7. Dose calculations of a proton beam passing through a virtual uniform water phantom with a titanium cylinder. Doses below 0.5% of the SOBP dose are not shown.

simulation reports a dose ~10% lower near the distal edge of the beam located behind the titanium cylinder.

The degradation of the end-of-range of the proton beam is also due to multiple Coulomb scattering,[28] and is not reproduced by the pencil-beam method.

III.B.4. Patient treatment plans

The analysis of the clinical proton beams reveals similar effects as seen in the phantom dose calculation. For example, shown in Fig. 8 are pencil-beam and Monte Carlo dose calculations of the posterior–anterior beam of the treatment plan for patient 1. Again, the Monte Carlo simulations show a large dose reduction distal to the implants and elevated dose distal to the edges of the hardware. The end-of-range of the beam is severely degraded; local range differences up to about 10 mm at 80% dose level are observed.

III.C. Overall impact on chordoma treatment plans

Dose distributions for the complete treatment plans of both patients are shown in Figs. 9 and 10. We compare the original dose calculations, using the pencil-beam algorithm and original CT images, with recalculations utilizing Monte Carlo simulation and artifact-reduced CT images. Dose–volume histograms are plotted in Fig. 11.

The use of several uniform proton beams reduced the impact of the dose errors on the overall treatment plan: although

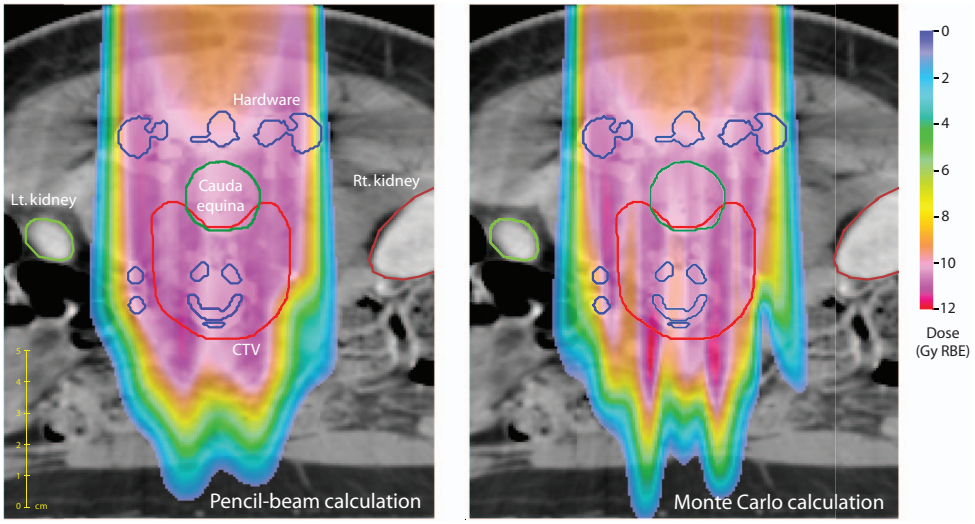

FIG. 8. Dose calculations of a posterior–anterior beam passing through titanium orthopedic hardware. Doses below 0.5 Gy RBE are not shown. CT window level: 40 HU and window width: 400 HU.

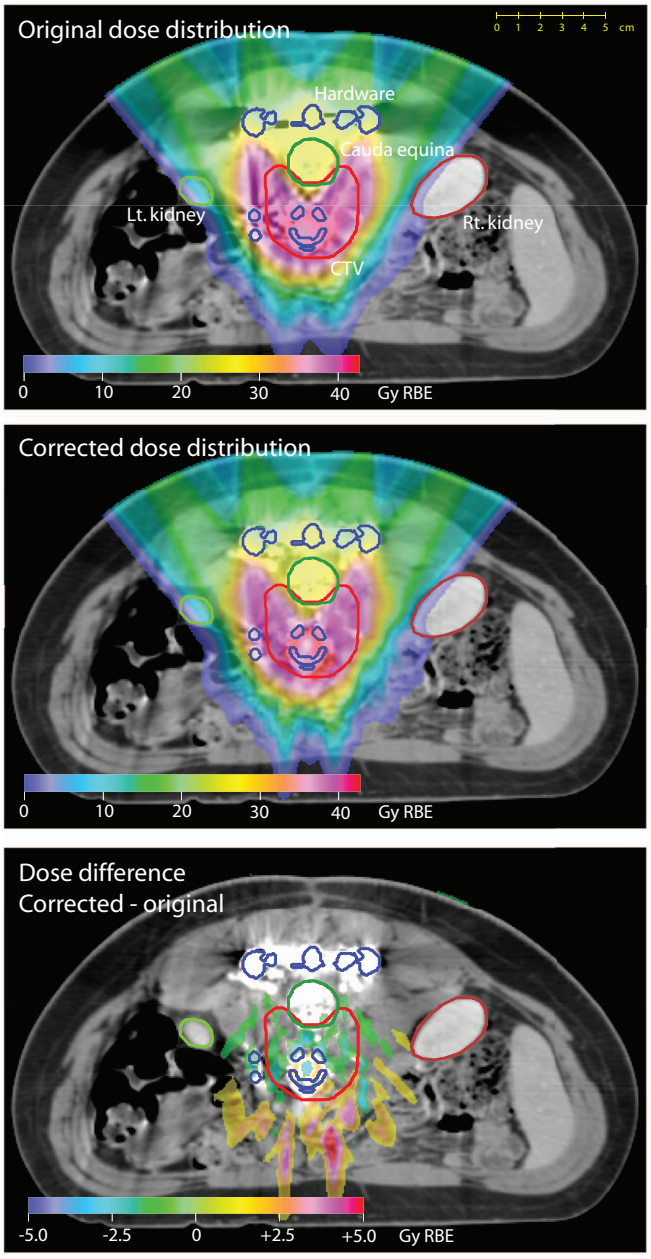

FIG. 9. Original and corrected dose distributions of the treatment plan of patient 1. The difference between the two dose calculations is also shown. Doses and dose differences below 1 Gy RBE are not displayed. CT window level: 40 HU and window width: 400 HU.

dose errors up to 10% of the SOBP dose were seen in the dose distributions of individual proton beams (refer Fig. 8), these errors were located at different positions for each beam, reducing the total impact on the treatment plan. Since the treatment plans for patient 1 and patient 2 employed 7 and 12 beams, respectively, the plans are quite robust against local dose errors in the individual fields.

The recalculations of the treatment plans show almost no difference in the mean dose to the clinical target volume (CTV). The homogeneity of the target dose is somewhat affected; in particular, the DVHs show a high-dose tail due to hot spots around the implants inside the CTV (refer Fig. 11). In both cases, the maximum dose to the CTV was ~4 Gy RBE

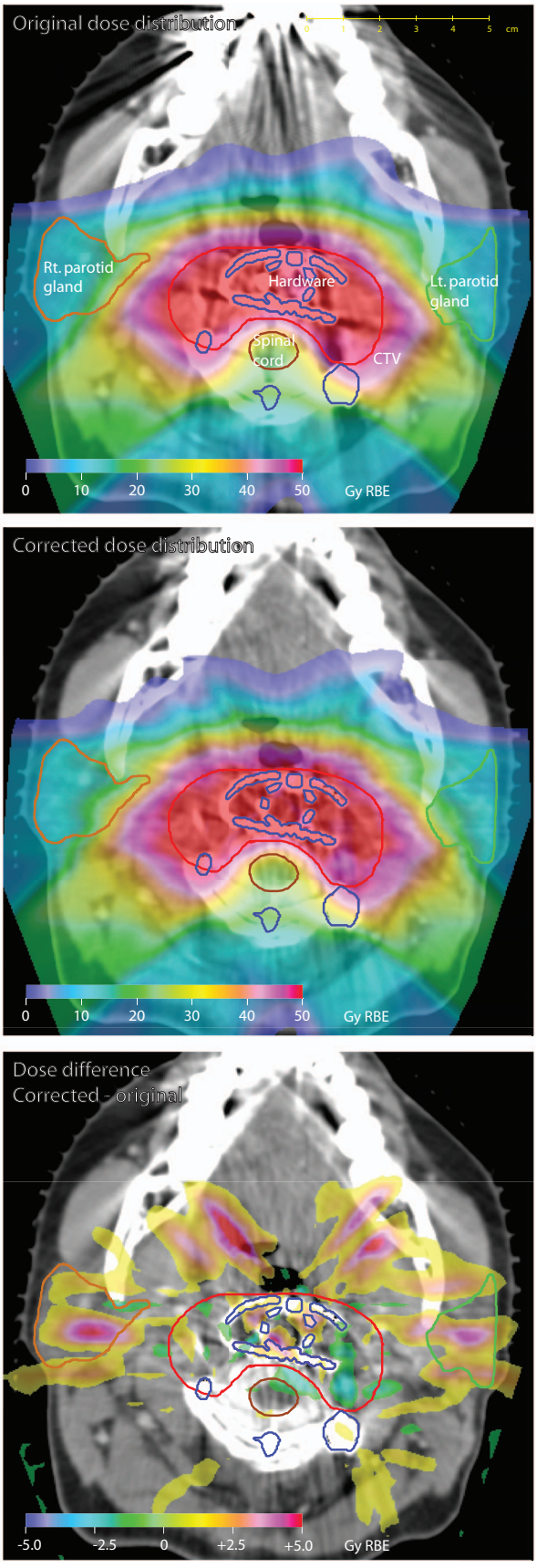

FIG. 10. Original and corrected dose distributions of the treatment plan of patient 2. The difference between the two dose calculations is also shown. Doses and dose differences below 1 Gy RBE are not displayed. CT window level: 40 HU and window width: 400 HU.

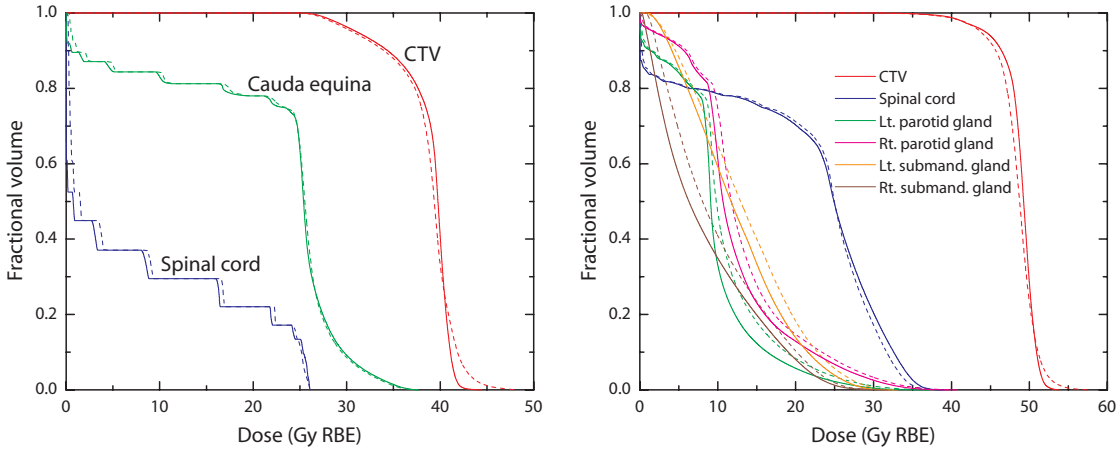

FIG. 11. Dose–volume histograms of the patient dose distributions. Solid lines: dose calculations on the original CT scans using the pencil-beam algorithm; dashed lines: dose recalculations using metal artifact reduction and Monte Carlo simulations.

higher in the recalculated dose distributions. In the case of patient 2, the mean dose to all salivary glands was increased by ~1 Gy RBE.

IV. DISCUSSION AND CONCLUSIONS

The purpose of this work was to investigate the dosimetric errors in clinical proton therapy dose calculation due to the presence of titanium implants, and to determine how these errors affect treatment of chordoma patients with orthopedic hardware.

We found that CT metal artifacts mainly affect the range of the proton beam, while the pencil-beam dose calculation algorithm underestimates dose inhomogeneity and range degradation distal to the implants.

The magnitude of the errors introduced by CT metal artifacts is highly dependent on the geometry of the hardware and the orientation of the proton beam relative to the artifacts. A phantom study showed range errors due to a severe metal artifact can vary between 1 and 10 mm. The evaluation of two chordoma cases, with titanium hardware around, respectively, the lumbar and cervical spine, showed mostly an underestimation of the proton range due to metal artifacts. Recalculations of the dose distributions on artifact-reduced CT scans revealed range increases up to 6 mm.

Second, the conventional pencil-beam dose calculation algorithms, which use water as a reference medium, do not consider effects specific to the nuclear structure of the irradiated materials. Also, scattering is calculated using the integrated radiological depth, which ignores the position of the implant in the beam path. We found that incomplete modeling of multiple Coulomb scattering results in the most significant errors, causing the dose delivered distal to typical titanium constructs to be overestimated by up to 10%. Proton range errors up to 10 mm occur in addition. The loss of proton fluence due to nonelastic nuclear reactions in the implant is reasonably estimated by the pencil-beam dose calculation, with dose errors being limited to about 1%. The result of these effects is that the characteristic "dose shadow" distal to titanium implants, as observed experimentally by Parodi *et al.*[3] and Schneider *et al.*,[29] is not well reproduced by the pencil-beam dose calculation.

The overall impact of dosimetric errors in the individual proton fields depends on the design of the treatment plan. The chordoma plans for passively scattered proton therapy were found to be quite robust against the errors introduced by the titanium implants. Dose recalculations which used artifact-reduced CT images and Monte Carlo simulations, showed only a small decrease in the homogeneity of the total dose delivered to the CTV. The mean dose to the CTV remained almost unchanged. This is mainly a result of the large number of proton beams used; since the errors due to the implants are generally at a different anatomical location in each proton field, the errors in the overall treatment plan tend to average out. Our results therefore do not show evidence for dosimetric inaccuracies in the treatment planning being a significant factor in the reduced tumor control of patients with titanium implants, which was reported by DeLaney *et al.*[5] and Staab *et al.*[4] It should however be noted that the patient group studied by Staab *et al.*[4] received spot scanning proton therapy, and the treatment design is therefore not directly comparable with the cases studied in this work. Also, analysis of a larger number of patients cases is needed to confirm these findings.

The dosimetric errors we identified apply in general to patients with titanium implants receiving proton therapy. Given the magnitude of the effects, we recommend to consider implementing methods to better estimate and mitigate the effects of the titanium implants.

Range errors due to CT metal artifacts can clearly be reduced using improved CT image reconstruction methods, which are starting to become commercially available. It is important to use a method that is designed to both provide an accurate segmentation of the high-density implants from

the surrounding tissue, and to reduce artifacts throughout the reconstructed CT images. Methods designed to improve diagnostic image quality should be separately validated to ensure accurate segmentation of the implant which is essential for dose calculation. Unless beams are oriented parallel to a metal artifact, our results show a trend towards range overshoot due to the bright artifacts directly surrounding the implants. CT metal artifact reduction would therefore be expected to potentially yield some reduction in dose to distal organs-at-risk such as the salivary glands. Because of range uncertainty in general, proton therapy treatment plans are normally designed with sufficient safety margins in the dose delivered to these organs.

The limitations of the pencil-beam dose calculation algorithm are a concern because dose inhomogeneity in the target is underestimated. While the physical interaction of the protons with the implants cannot be changed, an improved dose calculation algorithm that provides a good estimate of the effects can be helpful to determine how to mitigate them by changing the design of the treatment plan. Our results show that incorporating a better model of multiple Coulomb scattering would yield the most significant improvement. Potential methods to model this effect have previously been studied by Szymanowski and Oelfke[30] and Soukup *et al.*[31] Until such methods are implemented, one could account for the expected errors by using a larger number of beams and conservative range margins.

We believe that the design of future treatments for patients with titanium implants using intensity modulated proton therapy (IMPT) needs to be studied carefully. The advantages of robust optimization of IMPT treatment plans to account for uncertainties in the patient position and CT numbers are well known,[32] and are even more important in the case of patients with implants. However, if an IMPT plan is optimized without considering the limitations of the dose calculation algorithm, the possibility exists that a cold spot in the target volume as a result of multiple Coulomb scattering is not compensated for by other beams. Also, IMPT plans tend to require fewer beams to deliver highly conformal dose distributions, which would also increase the impact of the dosimetric errors on the overall treatment plan.

It should be mentioned that, in addition to the issues studied in this work, the image quality of the planning CT scan may also affect the accuracy of fusion of MRI images to the CT images for target and organ delineation. Also, artifacts may introduce errors in image guided patient setup using the CT scan as a reference. The impact of these effects has not yet been quantified.

To summarize, we found that dose calculations of proton beams in the presence of titanium implants are subject to significant errors due to CT metal artifacts and the incomplete model of multiple Coulomb scattering used by pencil-beam dose calculations. The overall treatment plans of chordoma patients, which employed passively scattered proton therapy, were however not as significantly affected. This is due to the local nature of the errors combined with the large number of fields, causing the errors to average out to a large degree.

ACKNOWLEDGMENTS

The authors would like to thank Tom Madden and Hanne Kooy, Ph.D., for providing the implementation of the pencil-beam dose calculation algorithm, and Jan Schümann, Ph.D., for the support of the TOPAS Monte Carlo code. Thanks to Juliane Daartz, Ph.D., for helpful feedback on the paper. This work was supported by the Federal Share of program income earned by Massachusetts General Hospital on C06-CA059267, Proton Therapy Research and Treatment Center.

[a]Author to whom correspondence should be addressed. Electronic mail: jverburg@fas.harvard.edu

[1]O. Jakel and P. Reiss, "The influence of metal artefacts on the range of ion beams," Phys. Med. Biol. **52**, 635–644 (2007).
[2]W. D. Newhauser, A. Giebeler, K. M. Langen, D. M. Mirkovic, and R. Mohan, "Can megavoltage computed tomography reduce proton range uncertainties in treatment plans for patients with large metal implants?," Phys. Med. Biol. **53**, 2327–2344 (2008).
[3]K. Parodi, H. Paganetti, E. Cascio, J. B. Flanz, A. A. Bonab, N. M. Alpert, K. Lohmann, and T. Bortfeld, "PET/CT imaging for treatment verification after proton therapy: A study with plastic phantoms and metallic implants," Med. Phys. **34**, 419–435 (2007).
[4]A. Staab, H. P. Rutz, C. Ares, B. Timmermann, R. Schneider, A. Bolsi, F. Albertini, A. Lomax, G. Goitein, and E. Hug, "Spot-scanning-based proton therapy for extracranial chordoma," Int. J. Radiat. Oncol., Biol., Phys. **81**, e489–e496 (2011).
[5]T. F. DeLaney, N. J. Liebsch, F. X. Pedlow, J. Adams, S. Dean, B. Y. Yeap, P. McManus, A. E. Rosenberg, G. P. Nielsen, D. C. Harmon, I. J. Spiro, K. A. Raskin, H. D. Suit, S. S. Yoon, and F. J. Hornicek, "Phase II study of high-dose photon/proton radiotherapy in the management of spine sarcomas," Int. J. Radiat. Oncol., Biol., Phys. **74**, 732–739 (2009).
[6]L. Hong, M. Goitein, M. Bucciolini, R. Comiskey, B. Gottschalk, S. Rosenthal, C. Serago, and M. Urie, "A pencil beam algorithm for proton dose calculations," Phys. Med. Biol. **41**, 1305–1330 (1996).
[7]J. M. Verburg and J. Seco, "CT metal artifact reduction method correcting for beam hardening and missing projections," Phys. Med. Biol. **57**, 2803–2818 (2012).
[8]M. R. Bussiere and J. A. Adams, "Treatment planning for conformal proton radiation therapy," Technol. Cancer Res. Treat. **2**, 389–399 (2003).
[9]M. Yang, X. R. Zhu, P. C. Park, U. Titt, R. Mohan, G. Virshup, J. E. Clayton, and L. Dong, "Comprehensive analysis of proton range uncertainties related to patient stopping-power-ratio estimation using the stoichiometric calibration," Phys. Med. Biol. **57**, 4095–4115 (2012).
[10]M. Urie, M. Goitein, and M. Wagner, "Compensating for heterogeneities in proton radiation-therapy," Phys. Med. Biol. **29**, 553–566 (1984).
[11]V. L. Highland, "Some practical remarks on multiple-scattering," Nucl. Instrum. Methods **129**, 497–499 (1975).
[12]B. Gottschalk, A. M. Koehler, R. J. Schneider, J. M. Sisterson, and M. S. Wagner, "Multiple Coulomb scattering of 160 MeV protons," Nucl. Instrum. Methods Phys. Res. B **74**, 467–490 (1993).
[13]J. Perl, J. Shin, J. Schümann, B. A. Faddegon, and H. Paganetti, "TOPAS—An innovative proton Monte Carlo platform for research and clinical applications," Med. Phys. **39**, 6818–6837 (2012).
[14]J. Allison, K. Amako, J. Apostolakis, H. Araujo, P. A. Dubois, M. Asai, G. Barrand, R. Capra, S. Chauvie, R. Chytracek, G. A. P. Cirrone, G. Cooperman, G. Cosmo, G. Cuttone, G. G. Daquino, M. Donszelmann, M. Dressel, G. Folger, F. Foppiano, J. Generowicz, V. Grichine, S. Guatelli, P. Gumplinger, A. Heikkinen, I. Hrivnacova, A. Howard, S. Incerti, V. Ivanchenko, T. Johnson, F. Jones, T. Koi, R. Kokoulin, M. Kossov, H. Kurashige, V. Lara, S. Larsson, F. Lei, O. Link, F. Longo, M. Maire, A. Mantero, B. Mascialino, I. McLaren, P. M. Lorenzo, K. Minamimoto, K. Murakami, P. Nieminen, L. Pandola, S. Parlati, L. Peralta, J. Perl, A. Pfeiffer, M. G. Pia, A. Ribon, P. Rodrigues, G. Russo, S. Sadilov, G. Santin, T. Sasaki, D. Smith, N. Starkov, S. Tanaka, E. Tcherniaev, B. Tome, A. Trindade, P. Truscott, L. Urban, M. Verderi, A. Walkden, J. P. Wellisch, D. C. Williams, D. Wright, and H. Yoshida, "Geant4 developments and applications," IEEE Trans. Nucl. Sci. **53**, 270–278 (2006).

[15]W. Schneider, T. Bortfeld, and W. Schlegel, "Correlation between CT numbers and tissue parameters needed for Monte Carlo simulations of clinical dose distributions," Phys. Med. Biol. **45**, 459–478 (2000).
[16]H. Paganetti, "Dose to water versus dose to medium in proton beam therapy," Phys. Med. Biol. **54**, 4399–4421 (2009).
[17]H. P. Wellisch and D. Axen, "Total reaction cross section calculations in proton-nucleus scattering," Phys. Rev. C **54**, 1329–1332 (1996).
[18]P. J. Bulman and J. A. R. Griffith, "Proton total reaction cross sections at 9.1 MeV," Nucl. Phys. A **111**, 315–3120 (1968).
[19]V. Meyer and N. M. Hintz, "Charged particle and total reaction cross sections for protons at 9.85 MeV," Phys. Rev. Lett. **5**, 207–209 (1960).
[20]B. D. Wilkins and G. Igo, "10-MeV proton reaction cross sections for several elements," Phys. Rev. **129**, 2198–2206 (1963).
[21]T. N. Nasr, A. M. Sourkes, D. J. Margaziotis, R. F. Carlson, and A. J. Cox, "Measurements of the total reaction cross section for protons on Ti and B between 20 and 50 MeV," Can. J. Phys. **56**, 56–62 (1978).
[22]W. Bauhoff, "Tables of reaction and total cross-section for proton nucleus scattering below 1 GeV," At. Data Nucl. Data Tables **35**, 429–447 (1986).
[23]NRG Petten, TALYS 1.4, 2012.
[24]A. J. Koning and J. P. Delaroche, "Local and global nucleon optical models from 1 keV to 200 MeV," Nucl. Phys. A **713**, 231–310 (2003).
[25]G. Molière, "Theorie der streuung schneller geladener teilchen II. Mehrfach- und vielfachstreuung," Z. Naturforsch. A **3**, 78–96 (1948).
[26]B. Gottschalk, BGware, version 04aug09, 2009.
[27]A. O. Hanson, L. H. Lanzl, E. M. Lyman, and M. B. Scott, "Measurement of multiple scattering of 15.7-MeV electrons," Phys. Rev. **84**, 634–637 (1951).
[28]G. O. Sawakuchi, U. Titt, D. Mirkovic, and R. Mohan, "Density heterogeneities and the influence of multiple Coulomb and nuclear scatterings on the Bragg peak distal edge of proton therapy beams," Phys. Med. Biol. **53**, 4605–4619 (2008).
[29]U. Schneider, P. Pemler, J. Besserer, M. Dellert, M. Moosburger, J. de Boer, E. Pedroni, and T. Boehringer, "The water equivalence of solid materials used for dosimetry with small proton beams," Med. Phys. **29**, 2946–2951 (2002).
[30]H. Szymanowski and U. Oelfke, "Two-dimensional pencil beam scaling: An improved proton dose algorithm for heterogeneous media," Phys. Med. Biol. **47**, 3313–3330 (2002).
[31]M. Soukup, M. Fippel, and M. Alber, "A pencil beam algorithm for intensity modulated proton therapy derived from Monte Carlo simulations," Phys. Med. Biol. **50**, 5089–5104 (2005).
[32]J. Unkelbach, T. Bortfeld, B. C. Martin, and M. Soukup, "Reducing the sensitivity of IMPT treatment plans to setup errors and range uncertainties via probabilistic treatment planning," Med. Phys. **36**, 149–163 (2009).